

# BEVScope: Enhancing Self-Supervised Depth Estimation Leveraging Bird’s-Eye-View in Dynamic Scenarios

Yucheng Mao<sup>1,2</sup>, Ruowen Zhao<sup>1,3</sup>, Tianbao Zhang<sup>1,4</sup> and Hang Zhao<sup>1\*</sup>

**Abstract**—Depth estimation is a cornerstone of perception in autonomous driving and robotic systems. The considerable cost and relatively sparse data acquisition of LiDAR systems have led to the exploration of cost-effective alternatives, notably, self-supervised depth estimation. Nevertheless, current self-supervised depth estimation methods grapple with several limitations: (1) the failure to adequately leverage informative multi-camera views. (2) the limited capacity to handle dynamic objects effectively. To address these challenges, we present BEVScope, an innovative approach to self-supervised depth estimation that harnesses Bird’s-Eye-View (BEV) features. Concurrently, we propose an adaptive loss function, specifically designed to mitigate the complexities associated with moving objects. Empirical evaluations conducted on the Nuscenes dataset validate our approach, demonstrating competitive performance. Code will be released at <https://github.com/myc634/BEVScope>.

## I. INTRODUCTION

In both the robotics and autonomous driving domains, the significance of 3D perception is paramount. Depth information, which acts as a vital link between 2D image inputs and the actual 3D environment, plays a crucial role [24, 6, 7]. However, the utilization of depth sensors, such as LiDAR, although effective, often faces obstacles owing to their significant cost and the relatively sparse nature of the data they provide. Conversely, cameras, despite lacking inherent depth information, present a cost-effective alternative that can capture an abundance of semantic information. Therefore, the challenge resides in the extraction of depth information from these 2D images, a task that depth estimation methodologies need to tackle effectively.

Owing to the significant cost associated with acquiring densely annotated depth maps, depth estimation often employs a self-supervised learning approach [30, 6, 37]. The pioneering technique of self-supervised monocular depth estimation was introduced by [37], which catalyzed a chain of subsequent advancements in this domain. The Full Surround Monodepth (FSM) [10] methodology expanded on this technique, integrating a multi-view perspective for the first time. Additional enhancements were brought about by SurroundDepth [30], which augmented the cross-view interaction of information via the implementation of Structure-from-Motion (SfM), consequently facilitating the recovery

of real-world scales. Multi-Camera Collaborative Depth Prediction (MCDP) [31] further propelled these advancements by introducing a depth consistency loss that refines depth information in regions captured by overlapping cameras. The prevalent methodology involves joint depth and pose prediction, which is utilized to map the target frame to the source frame, thereby computing photometric loss as the supervision signal. Nonetheless, this supervision signal may encounter challenges in addressing dynamic objects. However, they primarily concentrate on estimating depth from a camera view, resulting in a limited understanding of the geometric structure, which in turn hampers performance. Significant advancements have been observed in autonomous driving tasks such as object detection and map segmentation, owing to the incorporation of Bird’s-Eye-View (BEV) features [28, 14, 13, 17, 19, 32, 18, 24, 23, 20, 21, 15]. We advocate for the utilization of BEV features in fostering robust depth estimation methodologies. The proposed Bird’s-Eye-View (BEV)-oriented depth estimation strategy supersedes the conventional camera-view-dependent methods by explicitly integrating critical geometric structures. Our BEV-based approach is specifically devised to facilitate superior extraction and integration of geometric attributes across varied image perspectives. We delve into diverse techniques that drive the interaction between BEV information and image data.

To overcome the complexities associated with rapidly moving objects in real-world scenarios, we further present an adaptive loss function. In situations where a substantial number of rapidly moving objects persist within proximate frames of a given scene, this could lead to the ineffectiveness of self-supervised photometric loss in overseeing these rapid elements. The proposed adaptive photometric loss function is designed to lessen the weight according to rapidly moving objects within the supervision signal. Consequently, this promotes more robust and precise depth estimations.

In summary, our contributions are threefold:

(i) We introduce a novel depth estimation method that harnesses the power of Bird’s-Eye-View (BEV) features to integrate geometric cues, thereby enhancing self-supervised learning depth estimation. This proposal marks a first endeavor in the application of BEV features for depth map generation.

(ii) We introduce a novel loss function, tailored to address the complexities inherent in depth estimation for rapidly moving objects.

(iii) We evaluate our proposed method on popular multi-camera autonomous driving datasets and achieve a compet-

\*Corresponding at: [hangzhao@mail.tsinghua.edu.cn](mailto:hangzhao@mail.tsinghua.edu.cn).

<sup>1</sup>IIIS, Tsinghua University

<sup>2</sup>University of Science and Technology Beijing, 30 Xueyuan Road, Haidian District, Beijing, China. ([maoyucheng@xs.ustb.edu.cn](mailto:maoyucheng@xs.ustb.edu.cn))

<sup>3</sup>University of Chinese Academy of Sciences, 19 Yuquan Road, Shijingshan District, Beijing, China. ([zhaorewen20@mails.uicas.ac.cn](mailto:zhaorewen20@mails.uicas.ac.cn))

<sup>4</sup>Southeast University, No.2, Sipailou, Xuanwu District, Nanjing, China. ([tbzhangrobo@gmail.com](mailto:tbzhangrobo@gmail.com))

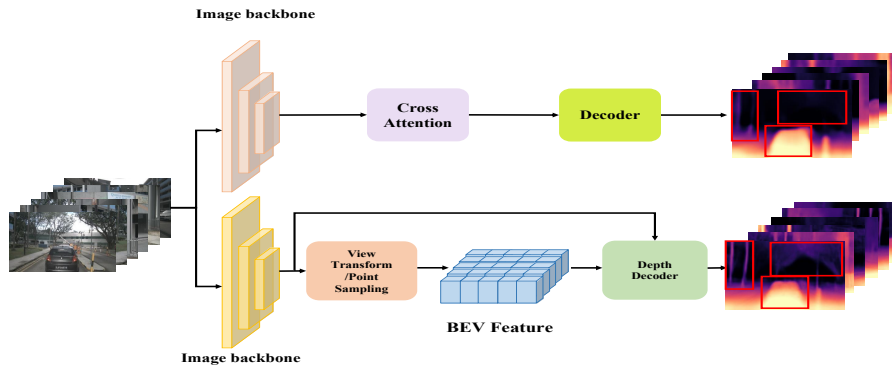


Fig. 1: Comparison of BEVScope and camera-view-based depth estimation methods. The upper workflow illustrates camera-view-based depth estimation method [30, 31, 10], which do not account for the geometric relationships between different perspective views. The lower workflow illustrates our proposed BEVScope method. **View Transform** signifies the BEV feature generation methods based on the LSS paradigm [14, 13, 17, 24, 23, 18]. Furthermore, **Point Sampling** refers to BEV feature generation methods that share similarities with [19, 32]

itive performance compared to the current state-of-the-art methods.

## II. RELATED WORK

### A. BEV-based Visual Perception

Bird’s Eye-View (BEV) in 3D perception has garnered considerable interest recently due to its capability to represent an entire scene by integrating multiple views of data captured from surrounding cameras. Contemporary methods for generating BEV features primarily fall into two categories: dense BEV-based methods [14, 13, 17, 19, 32, 18, 24, 23, 15] and sparse query-based methods [28, 20, 21, 22].

Dense BEV-based methods address transformation in a direct manner, with Lift-Splat-Shoot (LSS) [24] as a prime example of this approach. BEVDepth [17] and BEVDet [14] employ the LSS paradigm, proposing efficient frameworks for multi-camera 3D object detection from Bird’s Eye-View. BEVFormer [19] is the first to incorporate sequential temporal modeling into multi-view 3D object detection, implementing temporal self-attention. Building on its prior version, BEVDet4D [13] also exploits temporal cues from multi-camera images. Besides these methods that fuse short-term timestamp images to generate the BEV feature map, SOLOFusion [23] utilizes multiple timesteps across a long-term history.

Sparse query-based methods generally utilize learnable queries to aggregate 2D image features via an attention mechanism. DETR3D [28] initially leverages object queries to predict 3D positions, subsequently back-projecting them to 2D coordinates to extract the corresponding features. PETR [21], on the other hand, encodes 3D position information into the image features, enabling direct querying with global 2D features.

### B. Self-Supervised Monocular Depth Estimation

Existing methodologies for self-supervised monocular depth estimation concurrently utilize depth and motion networks. These apply a photometric consistency loss, altered by the

predicted depth and motion between target and source images [37, 8, 1, 35, 33, 29, 36, 26, 3]. Zhou et al. [37] were the pioneers in developing a self-supervised pipeline for the estimation of depth and ego-motion. Subsequent advancements by Godard et al. [7] incorporated a minimal reprojection loss to cater to occlusions, a full-resolution multi-scale sampling methodology to minimize visual artifacts, and a self-masking loss to disregard outlier pixels. A more recent approach, the PackNet SfM by Guizilini et al. [9], integrates packing and unpacking blocks that exploit 3D convolutions to acquire dense appearance and geometric data in real-time. This technique was further enhanced by Poggi et al. [25], who examined the estimation of uncertainty in this task and its effects on depth accuracy. Additionally, the Mono-Lite framework [34] introduces a hybrid CNN and Transformer structure, yielding superior accuracy compared to Monodepth2 [7] whilst reducing the model parameters. Despite the substantial advancements these works have brought to monocular depth estimation tasks, their extension to multi-view settings frequently encountered in autonomous driving scenarios is limited. Further, their capability to extract cross-view information effectively remains insufficient.

### C. Self-Supervised Surround-View Depth Estimation

Recent studies have sought to address these challenges in multi-view settings. Guizilini et al. [10] developed the Full Surround Monocular (FSM) approach, utilizing generalized spatio-temporal contexts and pose consistency constraints to facilitate self-supervised depth estimation with comprehensive surround multi-camera inputs. Similarly, the Surround-Depth methodology introduced by Wei et al. [30] intertwines surrounding visual information across multiple scales via a cross-view transformer, while a joint pose estimation framework fully exploits the extrinsics in multi-camera settings. Further, Xu et al. [31] put forth the Multi-Camera Depth Prediction (MCDP) methodology, which introduces a depth consistency loss for minimizing disparities in depth for overlapping areas between depth maps estimated from different

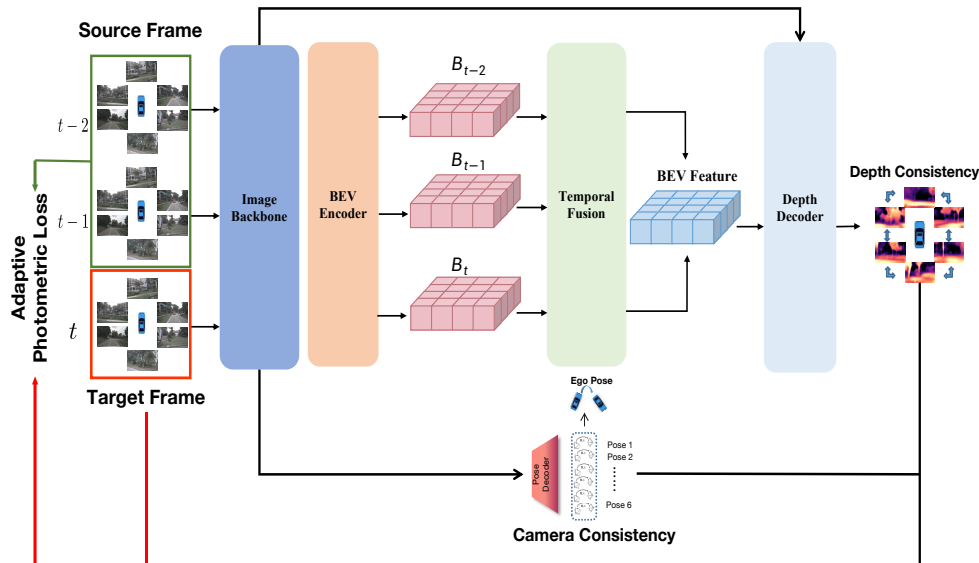


Fig. 2: The Architecture of BEVScope: Our proposed BEVScope architecture encompasses a meticulously crafted depth estimation task head that facilitates the prediction of dense depth maps by leveraging both the existing image features and BEV features. To bolster the precision of depth estimation, particularly for fast-moving objects, we introduce an adaptive photometric loss function. Furthermore, for the temporal fusion of BEV features, we integrate a camera pose consistency loss function. The **BEV Encoder** component denotes the BEV generating methods employed, such as [14, 13, 19]. The **Temporal Fusion** model indicate as the temporal fusion block used in [13, 19].

cameras. However, these methodologies predominantly rely on 2D feature extraction models, and as such, fail to fully leverage the powerful feature extraction capabilities of BEV-based visual perception frameworks.

### III. METHOD

#### A. Overview

In this work, we put forth a Bird’s-Eye-View (BEV)-based module designed for surround-view depth estimation. As depicted in Figure [2], our approach comprises of the BEV feature fusion module. The following sections will detail the definition of the surround view depth estimation task and elaborate on the underlying principles of the BEVScope approach.

#### B. Formulation

Considering two temporally sequential surround-view images,  $\mathbf{I}_i^t$  and  $\mathbf{I}_i^{t+1}$ , procured by multiple cameras  $\mathbf{C}_i$  (where  $i \in 1, 2, \dots, 6$  represents the number of cameras) encompassing a comprehensive view around a vehicle, our approach is tasked with estimating the depth  $\mathbf{D}_i^t$  and ego-motion  $\mathbf{P}_i^{t \rightarrow s}$  of each camera  $\mathbf{C}_i$ . We make the assumption that the camera intrinsics  $\mathbf{K}_i$  and extrinsics  $\mathbf{E}_i$  of each viewpoint are known factors.

The depth network denoted as  $F$  and the pose network represented by  $G$  are trained by minimizing a per-pixel photometric reprojection loss in a self-supervised manner [6, 37]. The formulation of surround-views depth estimation can be expressed as follows:

$$\mathbf{D}_i^t = F(\mathbf{I}_i^t), \quad \mathbf{P}_i^{t \rightarrow s} = G(\mathbf{I}_i^t, \mathbf{I}_i^s) \quad (1)$$

#### C. Depth Estimation Decoder

The architecture of our proposed depth estimation component within BEVScope is demonstrated in Figure[3].

**Network parameterization** Our proposed **Scope Head** is to predict the depth map in  $\mathbf{k}$ -scales from  $\mathbf{k}$ -scales feature maps and the BEV feature. We define  $F_{\text{img}}^k \in \mathbb{R}^{N \times H_{\text{img}}^k \times W_{\text{img}}^k \times C_{\text{img}}^k}$  to represent the feature map, extracted from the surround  $N$  cameras in  $\mathbf{k}$ -scales from a weight-sharing image backbone. We denote  $F_{\text{BEV}} \in \mathbb{R}^{1 \times H_{\text{BEV}} \times W_{\text{BEV}} \times C_{\text{BEV}}}$  as the BEV features generated from BEV encoder such as [14, 13, 19]. In our principal experiment, we utilize BEVFormer [19] as the BEV encoder. Here, we use  $T$  to represent our proposed depth estimation task head ( $i \in k$ ):

$$F_{\text{depth}}^i = T(F_{\text{img}}^i, F_{\text{BEV}}) \quad (2)$$

**Image-BEV Feature Fusion** Inspired by Vision Transformers [5], we transform the BEV features into patches. This transformation is based on the observation that feature maps from various perspective views display pronounced correlations with distinct regions in the BEV features. Specifically, we reshape the BEV feature  $F_{\text{BEV}} \in \mathbb{R}^{1 \times H_{\text{BEV}} \times W_{\text{BEV}} \times C_{\text{BEV}}}$  into a sequence of flattened 2D patches  $F_{\text{BEV}} \in \mathbb{R}^{1 \times N_{\text{BEV}} \times C_{\text{BEV}}}$  where  $(H_{\text{BEV}}, W_{\text{BEV}})$  defines the shape of the original BEV feature,  $(P_{\text{BEV}}, P_{\text{BEV}})$  determines the size of each BEV patch, and  $N = (H_{\text{BEV}} \times W_{\text{BEV}}) / P_{\text{BEV}}^2$  is the resulting quantity of patches.

TABLE I: Quantitative results for depth estimation on the nuScenes [2] dataset. All methods are trained and tested with the same experimental settings. † indicates that during the training process, we replace the images of adjacent frames in the keyframe with the images from adjacent frames in the sweeps of the nuScenes [2] dataset. \* indicates the implementation result in [30].

Methods	Abs Rel(↓)	Sq Rel(↓)	RMSE(↓)	a1(↑)	a2(↑)	a3(↑)
FSM[10]	0.299	-	-	-	-	-
FSM*[10]	0.334	2.845	7.786	0.508	0.761	0.894
SurroundDepth[30]	0.245	3.067	6.835	0.719	<b>0.878</b>	0.935
SurroundDepth†[30]	0.240	2.869	6.753	0.719	0.877	0.935
MCDP†[31]	0.237	3.030	6.822	0.719	-	-
BEVScope (w/o adaptive loss)	0.239	2.777	6.842	0.711	0.872	0.933
BEVScope†(w/o adaptive loss)	0.236	<b>2.122</b>	6.884	0.678	0.862	0.930
BEVScope†	<b>0.232</b>	2.652	<b>6.672</b>	<b>0.720</b>	0.876	<b>0.936</b>

Additionally, drawing on the Vision Transformer [5] approach, we consider the image feature as a token symbolizing the BEV feature, enabling effective combination of the two types of features. To mitigate computational cost associated with the quadratic term, following [30], we employ a depthwise separable convolution (DS-Conv) [4, 12] prior to image-BEV fusion layers to downsample the extensive feature maps into lower-resolution ones with same channel numbers, denoted as  $F_{\text{img}}^k \in \mathbb{R}^{N \times h_{\text{img}}^k \times w_{\text{img}}^k \times C_{\text{img}}^k}$ . We flatten the image feature from varying perspective views  $F_{\text{img}}^k \in \mathbb{R}^{N \times (h_{\text{img}}^k \times w_{\text{img}}^k) \times C_{\text{img}}^k}$  and concatenate the flattened image feature map with the BEV feature. The feature in each scale is formulated as follows, for  $i \in k$ :

$$F_{\text{all}}^i = \text{Concat}(F_{\text{img}}^i, F_{\text{BEV}}) \quad (3)$$

We then construct  $Z$  Image-BEV fusion self-attention layers with the objective of effectively integrating the two types of features. The image-BEV fusion layer is formulated as ( $i \in k$ ):

$$F_{\text{all}}^i = \text{Softmax}((F_{\text{all}}^i)^T F_{\text{all}}^i) / \sqrt{d_{F_{\text{all}}^i}} F_{\text{all}}^i \quad (4)$$

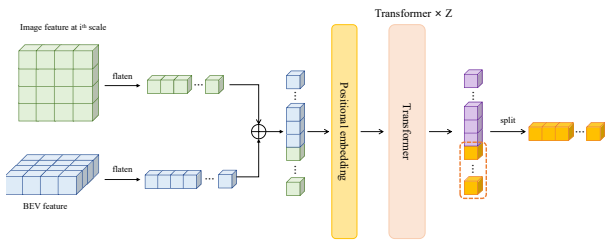


Fig. 3: Depth Head of BEVScope. For image feature map in each  $k$ -scales, we use DS-Conv to downsample it and concat with the flattened BEV feature. Then, we interact the image feature and BEV feature through a self-attention mechanism.

Upon completing the Image-BEV fusion layers, to restore the depth map from the fused feature, we split the  $F_{\text{all}}^i$  into

two sections, each corresponding to the original shape of  $F_{\text{img}}^i$  and  $F_{\text{BEV}}$ . We disregard the  $F_{\text{BEV}}$  and employ  $F_{\text{img}}^i$  to upsample to the original shape and predict the dense depth map.

While projecting the features from Bird’s-Eye-View (BEV) into different perspectives is a straightforward approach, it often results in sparse features that hinder effective up-sampling and accurate depth learning. To overcome this limitation, we propose a specially designed depth estimation task head to address this drawback.

#### D. Adaptive Photometric Loss Function for Fast Moving Objects

This section introduces a loss function with adaptive perception to ameliorate this issue.

**Traditional Photometric Loss** Traditionally, the supervision signal in a self-supervised depth estimation task is formulated as follows: Given a single image  $I_t$  input at the  $t$  frame, the system predicts its corresponding depth map  $D_t$ . Concurrently, the pose network leverages temporally adjacent images to estimate the relative pose  $T_{t \rightarrow t+n}$  between the target image  $I_t$  and the source image  $I_{t+n}$ . Based on the estimated depth map  $D_t$ , relative pose  $T_{t \rightarrow t+n}$ , and camera intrinsics matrix  $K$ , we can warp the image feature from the  $t$  frame to the  $t+n$  frame, denoted as  $I_{t \rightarrow t+n}$ . The system then minimizes the per-pixel minimum photometric re-projection error [6, 37]  $L_p$  as:

$$L_p = \min pe(I_t, I_{t+n \rightarrow t}) \quad (5)$$

where  $pe(\cdot)$  represents the photometric error, which consists of the  $L_1$  error and the Structural Similarity (SSIM):

$$pe(I_a, I_b) = \alpha (1 - \text{SSIM}(I_a, I_b)) + (1 - \alpha) |I_a - I_b|_1 \quad (6)$$

However, this supervision signal struggles with handling rapidly moving objects. Such objects may not maintain the same position in adjacent frames.

**Adaptive Photometric Loss Function** Hence, an adaptive loss function is proposed to tackle this problem. Specifically, we calculate the per-pixel SSIM value of adjacent frames  $I_t^i, I_t^s$ . This computation yields matrix  $S \in \mathbb{R}^{H \times W}$ , which is utilized as a weight when computing the photometric loss. The design intent here is to increase model focus on

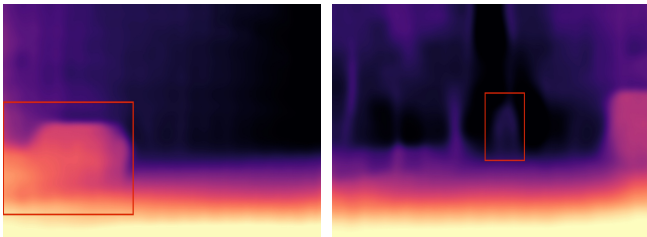
areas with smaller SSIM values between adjacent frames. Therefore, the difference between the identity matrix and the SSIM matrix  $(I - S) \in \mathbb{R}^{H \times W}$  is employed as the function weight. This approach effectively directs the network to pay less attention to areas with significant frame transitions. As a result, the adaptive loss function is reformulated as:

$$L_p^{ada} = (I - S)L_p \quad (7)$$

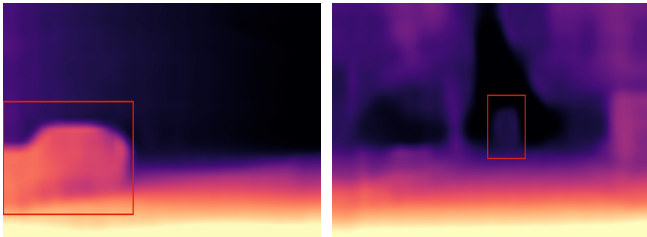
In the equation above,  $L_p$  denotes the original photometric loss.



(a) Original Image



(b) BEVScope(w/o adaptive mask)



(c) BEVScope(w adaptive mask)

Fig. 4: Demonstration of Adaptive Loss Function Effectiveness. We infer from the original image on BEVScope, comparing the results of two different scenarios: one using an adaptive loss function during training, and the other not. As illustrated by the contrast between Fig. (b) and Fig.(c), it is evident that the adaptive loss function improves the depth estimation for rapidly moving objects.

#### E. Incorporating Camera Pose Consistency

In observing prior methodologies [10], it was found that there was a lack of sufficient coupling between camera pose consistency and the task of depth estimation. This led to a lack of comprehensive attention to, and integration of, these two crucial aspects. To tackle this issue, we introduce an additional loss function, namely, a camera pose consistency constraint loss, which facilitates effective alignment of temporal BEV features. The benefit of this additional

loss function is that it strengthens the relationship between camera poses and depth estimation, thus enhancing the overall performance of the system.

The camera features are input to the pose decoder, which then predicts the pose for each camera, designated as  $P_i^{camera}$  where  $i \in 1, 2, \dots, 6$ .

The predicted camera poses at this stage are all situated in the coordinate system of their respective views. To impose an explicit constraint on the consistency across surround views, we transform the predicted camera poses into the ego coordinate system,  $P_i^{ego}$ , where  $i \in 1, 2, \dots, 6$ . Subsequently, we constrain the l1 norm of the vehicle’s ego pose,  $P_i^{ego}$ .

$$L_{pose} = \|P_i^{ego}\|_1, \quad i \in 1, 2, \dots, 6 \quad (8)$$

The final loss function for our model is then given by:

$$L_{final} = L_p^{ada} + L_{pose} + L_{depth} \quad (9)$$

In the above,  $L_p^{ada}$  refers to the adaptive photometric loss function,  $L_{pose}$  corresponds to the proposed ego pose loss, and  $L_{depth}$  denotes the depth consistency loss, as described in [31].

## IV. EXPERIMENTS

This section provides a comparative analysis of our proposed methodology with existing state-of-the-art self-supervised surround-view depth estimation techniques [cite] on the nuScenes [2] datasets. Additionally, an ablation study is conducted to ascertain the performance of various aspects of our proposed method. Visual results of fast-moving objects as predicted by our BEVScope and other leading depth estimation methods are also presented for clarity.

### A. Experimental Procedure

Our experiments employ depth and pose networks that share the same backbone structure as the Monodepth2 model [7]. Specifically, we utilize the ResNet34 [11] with ImageNet [27] pretrained weights as the encoder for all experiments in line with the SurroundDepth approach [30], inclusive of baseline methods. The depth maps were refactored based on varying focal lengths of the surrounding cameras, as detailed in [16]. We incorporated  $Z = 8$  image-BEV fusion layers for each scale, with all features downsampled to a  $15 \times 10$  size prior to BEV fusion across both datasets. For a fair comparison with SurroundDepth and MCDP techniques, we used the same sweeps data from the nuScenes dataset as employed in the MCDP method [31].

### B. Ablation Study

This subsection presents the results of the ablation studies conducted to validate the effectiveness of individual modules within our proposed framework. All experiments were executed on the nuScenes dataset.

**Evaluation of BEV Feature Generation Techniques:** We conducted a series of experiments employing diverse BEV generation techniques [14, 13, 19] to evaluate the adaptability

of our proposed task head. Table II presents the performance of our task head using various BEV feature generation methods.

TABLE II: Ablation Study of Depth Estimation with Different BEV Feature Generation Techniques

Methods	Abs Rel( $\downarrow$ )	Sq Rel( $\downarrow$ )	RMSE( $\downarrow$ )	a1( $\uparrow$ )
BevDet [14]	0.250	2.876	7.119	0.689
BevDet4D [13]	0.248	2.682	7.070	0.713
BEVFormer [19]	<b>0.232</b>	<b>2.652</b>	<b>6.672</b>	<b>0.720</b>

**Adaptive Loss Function:** Fig. 4 visually demonstrates the effectiveness of the adaptive loss function in handling fast-moving objects. Additionally, Table III evaluates our model with and without the adaptive loss function on scenes containing fast-moving objects, highlighting the significance of this approach. Notably, we have selected the scenes which contain more than one fast-moving objects in the nuScenes [2] validation set for evaluation.

TABLE III: Ablation Study For Adaptive Loss Function

Methods	Abs Rel( $\downarrow$ )	Sq Rel( $\downarrow$ )	RMSE( $\downarrow$ )	a1( $\uparrow$ )
w/o adaptive loss	0.230	<b>2.142</b>	7.178	0.684
with adaptive loss	<b>0.226</b>	2.685	<b>6.985</b>	<b>0.728</b>

**Camera Consistency Loss Function:** Table IV shows the effectiveness of the camera consistency loss function in aligning the BEV feature in the temporal BEV generating method.

TABLE IV: Ablation Study For Camera Consistency Loss Function (cam consis. refer to camera consistency)

Methods	Abs Rel( $\downarrow$ )	Sq Rel( $\downarrow$ )	RMSE( $\downarrow$ )	a1( $\uparrow$ )
w/o cam consis.	0.246	3.696	7.273	0.729
with cam consis.	<b>0.232</b>	<b>2.652</b>	<b>6.672</b>	<b>0.720</b>

**Patch Embedding on BEV Feature:** Table V illustrate the importance of patch embedding

TABLE V: Ablation Study For Patch Embedding on BEV Feature

Methods	Abs Rel( $\downarrow$ )	Sq Rel( $\downarrow$ )	RMSE( $\downarrow$ )	a1( $\uparrow$ )
w/o patch embedding	0.248	3.46	7.192	0.727
with patch embedding	<b>0.232</b>	<b>2.652</b>	<b>6.672</b>	<b>0.720</b>

## V. CONCLUSIONS

In this paper, we propose a self-supervised multi-camera depth estimation method named **BEVScope**. We leverage the advantages of BEV features in fusing multi-view information, while introducing new constraints to address the complexity of joint pose estimation and mutual consistency in multi view depth maps by fully utilizing the camera consistency and adaptive Loss Function. Our method achieves competitive performance on multi camera depth estimation datasets, such as NuScenes[2] datasets.

## REFERENCES

- [1] Jia-Wang Bian et al. “Unsupervised Scale-consistent Depth and Ego-motion Learning from Monocular Video”. In: *NeurIPS*. 2019, pp. 35–45.
- [2] Holger Caesar et al. “nusScenes: A multimodal dataset for autonomous driving”. In: *Proceedings of the IEEE/CVF conference on computer vision and pattern recognition*. 2020, pp. 11621–11631.
- [3] Jia-Ren Chang and Yong-Sheng Chen. “Pyramid stereo matching network”. In: *CVPR*. 2018, pp. 5410–5418.
- [4] François Chollet. “Xception: Deep learning with depthwise separable convolutions”. In: *Proceedings of the IEEE conference on computer vision and pattern recognition*. 2017, pp. 1251–1258.
- [5] Alexey Dosovitskiy et al. “An image is worth 16x16 words: Transformers for image recognition at scale”. In: *arXiv preprint arXiv:2010.11929* (2020).
- [6] Clément Godard, Oisín Mac Aodha, and Gabriel J Brostow. “Unsupervised monocular depth estimation with left-right consistency”. In: *Proceedings of the IEEE conference on computer vision and pattern recognition*. 2017, pp. 270–279.
- [7] Clément Godard et al. “Digging into self-supervised monocular depth estimation”. In: *Proceedings of the IEEE/CVF international conference on computer vision*. 2019, pp. 3828–3838.
- [8] Clément Godard et al. “Digging into self-supervised monocular depth estimation”. In: *ICCV*. 2019, pp. 3828–3838.
- [9] Vitor Guizilini et al. “3d packing for self-supervised monocular depth estimation”. In: *Proceedings of the IEEE/CVF conference on computer vision and pattern recognition*. 2020, pp. 2485–2494.
- [10] Vitor Guizilini et al. “Full surround monodepth from multiple cameras”. In: *IEEE Robotics and Automation Letters* 7.2 (2022), pp. 5397–5404.
- [11] Kaiming He et al. “Deep residual learning for image recognition”. In: *Proceedings of the IEEE conference on computer vision and pattern recognition*. 2016, pp. 770–778.
- [12] Andrew G. Howard et al. *MobileNets: Efficient Convolutional Neural Networks for Mobile Vision Applications*. 2017. arXiv: 1704.04861 [cs.CV].
- [13] Junjie Huang and Guan Huang. “Bevdet4d: Exploit temporal cues in multi-camera 3d object detection”. In: *arXiv preprint arXiv:2203.17054* (2022).
- [14] Junjie Huang et al. “Bevdet: High-performance multi-camera 3d object detection in bird-eye-view”. In: *arXiv preprint arXiv:2112.11790* (2021).
- [15] Yanqin Jiang et al. “Polarformer: Multi-camera 3d object detection with polar transformers”. In: *arXiv preprint arXiv:2206.15398* (2022).
- [16] Jin Han Lee et al. “From big to small: Multi-scale local planar guidance for monocular depth estimation”. In: *arXiv preprint arXiv:1907.10326* (2019).

- [17] Yin hao Li et al. “Bevdepth: Acquisition of reliable depth for multi-view 3d object detection”. In: *arXiv preprint arXiv:2206.10092* (2022).
- [18] Yin hao Li et al. “Bevstereo: Enhancing depth estimation in multi-view 3d object detection with dynamic temporal stereo”. In: *arXiv preprint arXiv:2209.10248* (2022).
- [19] Zhiqi Li et al. “Bevformer: Learning bird’s-eye-view representation from multi-camera images via spatiotemporal transformers”. In: *Computer Vision–ECCV 2022: 17th European Conference, Tel Aviv, Israel, October 23–27, 2022, Proceedings, Part IX*. Springer, 2022, pp. 1–18.
- [20] Xuewu Lin et al. “Sparse4D: Multi-view 3D Object Detection with Sparse Spatial-Temporal Fusion”. In: *arXiv preprint arXiv:2211.10581* (2022).
- [21] Yingfei Liu et al. “Petr: Position embedding transformation for multi-view 3d object detection”. In: *Computer Vision–ECCV 2022: 17th European Conference, Tel Aviv, Israel, October 23–27, 2022, Proceedings, Part XXVII*. Springer, 2022, pp. 531–548.
- [22] Yingfei Liu et al. “Petrv2: A unified framework for 3d perception from multi-camera images”. In: *arXiv preprint arXiv:2206.01256* (2022).
- [23] Jinhung Park et al. “Time will tell: New outlooks and a baseline for temporal multi-view 3d object detection”. In: *arXiv preprint arXiv:2210.02443* (2022).
- [24] Jonah Philion and Sanja Fidler. “Lift, splat, shoot: Encoding images from arbitrary camera rigs by implicitly unprojecting to 3d”. In: *Computer Vision–ECCV 2020: 16th European Conference, Glasgow, UK, August 23–28, 2020, Proceedings, Part XIV 16*. Springer, 2020, pp. 194–210.
- [25] Matteo Poggi et al. “On the uncertainty of self-supervised monocular depth estimation”. In: *Proceedings of the IEEE/CVF Conference on Computer Vision and Pattern Recognition*. 2020, pp. 3227–3237.
- [26] Anurag Ranjan et al. “Competitive Collaboration: Joint Unsupervised Learning of Depth, Camera Motion, Optical Flow and Motion Segmentation”. In: *CVPR*. 2019, pp. 12240–12249.
- [27] Olga Russakovsky et al. “Imagenet large scale visual recognition challenge”. In: *IJCV* 115.3 (2015), pp. 211–252.
- [28] Yue Wang et al. “Detr3d: 3d object detection from multi-view images via 3d-to-2d queries”. In: *Conference on Robot Learning*. PMLR, 2022, pp. 180–191.
- [29] Zhongdao Wang et al. “Orientation invariant feature embedding and spatial temporal regularization for vehicle re-identification”. In: *ICCV*. 2017, pp. 379–387.
- [30] Yi Wei et al. “SurroundDepth: entangling surrounding views for self-supervised multi-camera depth estimation”. In: *Conference on Robot Learning*. PMLR, 2023, pp. 539–549.
- [31] Jialei Xu et al. “Multi-Camera Collaborative Depth Prediction via Consistent Structure Estimation”. In: *Proceedings of the 30th ACM International Conference on Multimedia*. 2022, pp. 2730–2738.
- [32] Chenyu Yang et al. “BEVFormer v2: Adapting Modern Image Backbones to Bird’s-Eye-View Recognition via Perspective Supervision”. In: *Proceedings of the IEEE/CVF Conference on Computer Vision and Pattern Recognition*. 2023, pp. 17830–17839.
- [33] Zhichao Yin and Jianping Shi. “Geonet: Unsupervised learning of dense depth, optical flow and camera pose”. In: *CVPR*. 2018, pp. 1983–1992.
- [34] Ning Zhang et al. “Lite-mono: A lightweight cnn and transformer architecture for self-supervised monocular depth estimation”. In: *Proceedings of the IEEE/CVF Conference on Computer Vision and Pattern Recognition*. 2023, pp. 18537–18546.
- [35] Wang Zhao et al. “Towards Better Generalization: Joint Depth-Pose Learning without PoseNet”. In: *CVPR*. 2020.
- [36] Junsheng Zhou et al. “Moving Indoor: Unsupervised Video Depth Learning in Challenging Environments”. In: *ICCV*. 2019, pp. 8618–8627.
- [37] Tinghui Zhou et al. “Unsupervised learning of depth and ego-motion from video”. In: *CVPR*. 2017, pp. 1851–1858.

## VI. APPENDIX

### A. Datasets

We conduct our experiments on NuScenes Dataset [2], which is composed of 1000 sequences of outdoor scenes in Boston and Singapore and each sequence has an approximate duration of 20 seconds. The dataset is officially partitioned into training, validation, and testing subsets, comprising 700, 150, and 150 sequences respectively. In each sample, we have access to the six surrounding cameras along with their corresponding calibrations and neighbour frame information [30].

### B. Implementation Details

We train all models with 5 epochs and a batch size of 1, where each batch contains 6 multi-view images, per NVIDIA RTX 3090 GPU. In line with the previous work, specially monodepth2[7], we set SSIM weight to 0.85 and L1 weight to 0.15 respectively in the reprojection loss. Furthermore, we assign a depth smooth weight of  $1e-3$  to ensure smoothness in the depth maps. In addition to these settings, we introduce our proposed constraints. We set both camera consistency and depth consistency loss weight as  $1e-4$  to enforce the consistency between the estimated camera poses and depth maps.

### C. Metrics

Self-supervised depth estimation models are typically evaluated using various metrics to assess the quality and accuracy of depth predictions. The following are some used evaluation metrics for our work:

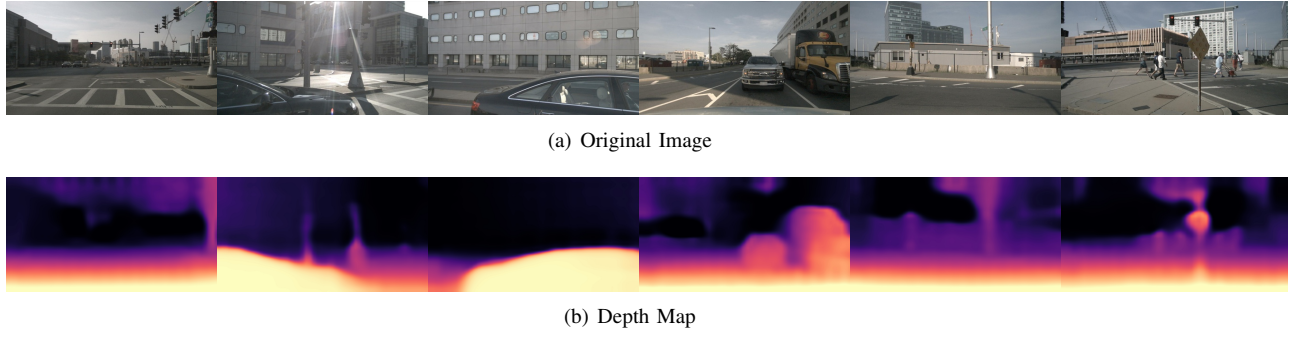


Fig. 5: Qualitative results on nuScenes[2] datasets.

$$AbsRel : \frac{1}{N} \sum_{i=1}^N \frac{|d_i - \hat{d}_i|}{d_i}$$

$$SqRel : \frac{1}{N} \sum_{i=1}^N \left( \frac{d_i - \hat{d}_i}{d_i} \right)^2$$

$$RMSE : \sqrt{\frac{1}{N} \sum_{i=1}^N (d_i - \hat{d}_i)^2}$$

$$RMSE_{log} : \sqrt{\frac{1}{N} \sum_{i=1}^N (\log d_i - \log \hat{d}_i)^2}$$

where  $N$  indicates the total number of pixels in a depth image  $D$ .  $d_i$  and  $\hat{d}_i$  respectively refer to groundtruth and predicted depth in  $i^{th}$  pixel. During the evaluation process,  $\frac{median(\hat{D})}{median(D)}$  is typically utilized as a factor to align the scale.

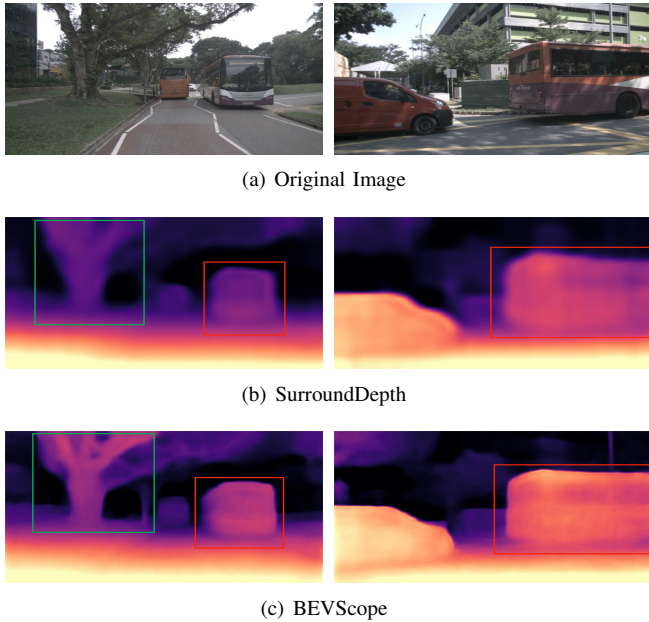


Fig. 6: Comparison of visualization result between Surrounddepth[30], and the proposed BEVScope.

#### D. Visualization and Comparison

The Figure [5] is qualitative results on nuScenes[2] dataset. As depicted in Figure [6], we present a qualitative visualization comparison between our model and Surround-Depth. Leveraging robust geometric cues in Bird’s Eye View (BEV) features and effective consistency constraints, our model demonstrates remarkable accuracy in generating depth maps. Additionally, we evaluate the prediction outcomes of BEVScope with and without the adaptive mask, as illustrated in Figure [7]. The inclusion of the adaptive mask results in more precise depth estimation, particularly for rapidly moving vehicles.

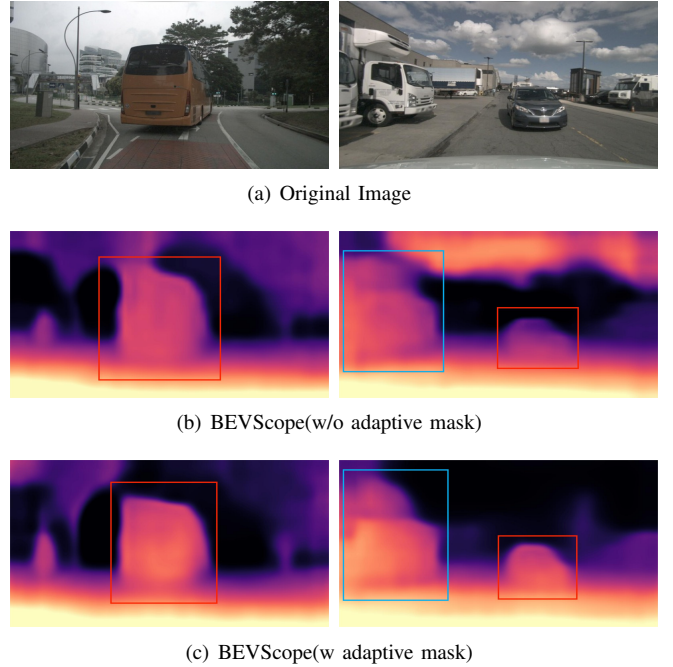


Fig. 7: Comparison between with the adaptive mask and without adaptive mask.